

Atmospheric CO₂ Column Measurements with an Airborne Intensity-Modulated Continuous-Wave 1.57-micron Fiber Laser Lidar

**Jeremy T. Dobler^{1*}, F. Wallace Harrison², Edward V. Browell², Bing Lin², Doug
McGregor¹ Susan Kooi³, Yonghoon Choi³, and Syed Ismail²**

¹Exelis, Inc., 1919 W. Cook Rd., Ft. Wayne, IN 46818 USA

*²National Aeronautics and Space Administration, Langley Research Center, Hampton, VA 23681
USA*

³Science Systems and Applications Inc., 1 Enterprise Pkwy, Hampton, VA 23666 USA

**Corresponding author: Jeremy.Dobler@exelisinc.com*

Abstract

The 2007 National Research Council (NRC) Decadal Survey on Earth Science and Applications from Space recommended Active Sensing of CO₂ Emissions over Nights, Days, and Seasons (ASCENDS) as a mid-term, Tier II, NASA space mission. ITT Exelis, formerly ITT Corp., and NASA Langley Research Center have been working together since 2004 to develop and demonstrate a prototype Laser Absorption Spectrometer for making high-precision, column CO₂ mixing ratio measurements needed for the ASCENDS mission. This instrument, called the Multifunctional Fiber Laser Lidar (MFLL), operates in an intensity-modulated, continuous-wave mode in the 1.57- μm CO₂ absorption band. Flight experiments have been conducted with the MFLL on a Lear-25, UC-12, and DC-8 aircraft over a variety of different surfaces and under a

wide range of atmospheric conditions. Very high-precision CO₂ column measurements resulting from high signal-to-noise (>1300) column optical depth measurements for a 10-s (~ 1 km) averaging interval have been achieved. *In situ* measurements of atmospheric CO₂ profiles were used to derive the expected CO₂ column values, and when compared to the MFLM measurements over desert and vegetated surfaces, the MFLM measurements were found to agree with the *in situ*-derived CO₂ columns to within an average of 0.17% or ~0.65 ppmv with a standard deviation of 0.44% or ~1.7 ppmv. Initial results demonstrating ranging capability using a swept modulation technique are also presented.

1. Introduction

Our ability to model accurately future climate change is directly associated with improving our understanding of the processes determining atmospheric CO₂ levels. According to the Intergovernmental Panel on Climate Change (IPCC) fourth assessment report (FAR) [1], more than 50 percent of the CO₂ released by fossil-fuel combustion and land-use change remains in the atmosphere with the oceans and land sequestering the other half of the CO₂; however, the uncertainties associated with CO₂ in land-use change and land sequestration is exceedingly large (over 70 percent of their budgets), while the uncertainty in the ocean budget is estimated to be about 25 percent. In addition, all of the sources and sinks for atmospheric CO₂ have large, regional and temporal variability and need to be studied over regional scales to address a global issue such as climate change.

The U.S. National Research Council's report entitled *Earth Science and Applications from Space: National Imperatives for the Next Decade and Beyond* identified the need for a mid-term space mission of Active Sensing of CO₂ Emissions over Nights, Days, and Seasons (ASCENDS)

to address the need for a better understanding of global sources and sinks of CO₂ [2]. The primary objective of the ASCENDS mission is to make Integrated Path Differential Absorption (IPDA) lidar CO₂ measurements across the mid-lower troposphere during day and night, over all latitudes, all seasons, and in the presence of thin or scattered clouds. These measurements will be used to significantly reduce the uncertainties in global estimates of CO₂ sources and sinks, to provide an increased understanding of the connection between climate and CO₂ exchange, to improve climate models, and to close the carbon budget for improved climate forecasting and policy decisions.

The ASCENDS mission requires an active sensor that satisfies the required CO₂ column measurement precision and accuracy from space in order to determine the global variability of CO₂ across the troposphere and thereby determine regional CO₂ sources and sinks at the surface. The critical component in the ASCENDS mission is the Laser Absorption Spectrometer (LAS), which is used for making IPDA CO₂ column measurements with preferential weighting to the mid to lower troposphere. ITT Exelis developed an airborne demonstration unit in 2004 and has been working with NASA Langley Research Center (LaRC) since 2005 to improve and evaluate the prototype LAS instrument for global CO₂ measurements from space. This instrument, called the Multifunctional Fiber Laser Lidar (MFLL), operates in an intensity-modulated, continuous-wave (IM-CW) mode in the 1.57- μm CO₂ absorption region [3]. The laser technology used in the MFLL is leveraged from the telecommunications industry and has the benefits of efficient operation, sealed components, and long lifetimes. In addition, this technology is compact and can be scalable to meet the requirements of the ASCENDS mission.

Diode lasers operating at discrete wavelengths on and off the CO₂ absorption line at 1571.112 nm are intensity-modulated at different frequencies and combined and amplified

simultaneously in a single erbium-doped fiber amplifier (EDFA). The amplified on-line and off-line modulated laser beams are transmitted to the atmosphere simultaneously and the backscattered returns from the Earth's surface, as well as clouds and aerosols, are collected with a single detector. The simultaneous transmission of the two laser wavelengths within the same beam eliminates common mode errors in the IPDA CO₂ column measurements that can result from a mismatch in the sampled atmospheric volume/scattering surface between the on-line and off-line backscattered returns. The backscattered signals from the surface or cloud tops are collected simultaneously by the receiver system, and using an analytical lock-in technique, the independent signals at the transmitted wavelengths are uniquely separated for the IPDA CO₂ column measurement [4].

The MFLC began flight evaluation in 2005, and since then it has flown in ten flight-test campaigns on three different aircraft: Lear-25 (2005-2007, 5 campaigns), NASA UC-12 (2008-2011, 5 campaigns), and NASA DC-8 (2010-2011, 2 campaigns). Measurements of CO₂ columns were made over a large range of altitudes during day and night, over different types of land and ocean surfaces, and in clear and partly cloudy conditions, which are all requirements of the ASCENDS mission. On the early flight tests the MFLC CO₂ column measurements were found to have very high signal-to-noise ratio's (SNR) exceeding 600 in certain cases, demonstrating a CO₂ measurement precision of ~ 0.6 ppm over a 1-s (~ 100 m) integration period [5] [6].

The initial MFLC operations utilized unique fixed modulation frequencies in the 50 kHz range; however, due to the ubiquitous nature of cirrus clouds for the ASCENDS mission, it was necessary to go to a variable modulation frequency technique to provide range discrimination in the MFLC CO₂ measurement. A swept modulation frequency approach [7] over the range of

100-600 kHz was used in MFL CO₂ column measurements during 2011 UC-12 and DC-8 flight tests [8][9]. Comparisons between MFL remotely sensed CO₂ columns and *in situ*-derived CO₂ columns demonstrated the absolute accuracy of the MFL measurements to within ~0.65 ppm.

In this paper, a brief overview of the IPDA technique used by the MFL LAS system is discussed and an overview of the MFL instrument is presented. A discussion of the signal processing used to retrieve the lidar signals is presented next. This is followed by a detailed discussion of the MFL CO₂ precision and accuracy measurement results from recent flight tests. Examples of range measurement capability to cloud layers and the surface are also presented.

2. Theory of IPDA Technique

Accurate measurements of atmospheric column amounts of CO₂ are critical to gain advanced knowledge of CO₂ global distributions and its variations. Analyses [10][11] found that global measurements of the column CO₂ with the accuracy of a few ppm would significantly reduce the uncertainty of CO₂ sources and sinks. The global CO₂ measurements could be achieved using the IPDA technique [12][13][14] that measures the difference of gas absorption integrated along the entire vertical path of two or more spectrally narrow wavelengths of light. The wavelengths are very closely spaced and are selected appropriately around the absorption feature of interest, with at least one of the lines being in the absorption feature and at least one line off of the absorption feature. For airborne systems, the wavelength may be selected on the absorption line center (called on-line) and in the far wings (or off-lines) to maximize differential absorption between on-line and off-lines. Due to the close proximity of the transmitted wavelengths (<100 pm separation), differences in the reflectivity, backscatter coefficients and the absorption of most atmospheric gases except CO₂ and H₂O are negligible. Optimal selection

of wavelengths can also render the H₂O absorption differences between the on-line and off-line negligible as well, thus allowing the differential absorption technique to isolate the CO₂ gas absorption from the influences of backscatters and absorption of other gases [12][13][14].

At present, global column CO₂ measurements are obtained from satellite passive remote sensing techniques [11][15][16][17]. These passive remote sensing techniques generally include measurements of atmospheric thermal emission and reflection of solar light at visible (VIS) and near infrared (NIR) wavelengths. Lack of sensitivity of thermal emission methods to the lower troposphere where most of the atmospheric CO₂ exists and actively interacts with its sources and sinks is a major concern of this kind of measurement [18]. For passive VIS-NIR satellite measurements [11][12][18], IPDA technique would provide reasonable precision of CO₂ estimates around 1 - 10 ppm [10]. However, this kind of technique is fully dependent on solar radiation, and only daytime measurements are available. Furthermore, passive approaches have relatively large footprints and are susceptible to bias due to interference from clouds and aerosols which alter the column path length. The ASCENDS mission requires observations of CO₂ distributions during both day and night and over all seasons and latitudes, which requires an active measurement approach. Various active remote sensing methods using laser IPDA techniques have been proposed and analyzed [3][5][19-25]. Here, we give a brief discussion of the IM-CW laser based IPDA technique. For a detailed description see for example “Laser Remote Sensing: Fundamentals and Applications” [13].

For simplicity, we first present the standard lidar equation for the received signal power P_{rec} at wavelength λ_0 from a volumetric scattering target of ΔR , centered at range R , given by:

$$P_{rec}(\lambda_0, R) = P_L \frac{A_0}{R^2} * \eta(\lambda_0) * \xi(R_T) * \beta_\pi(\lambda_L, R) * \Delta R * \exp \left[-2 \int_0^R \kappa(\lambda_0, r) dr \right] \quad (1)$$

where P_L is the transmitted laser power, $\frac{A_0}{R^2}$ is the solid angle subtended by the receiver, $\eta(\lambda_0)$ is the optical efficiency of the receiver system at λ_0 , $\xi(R)$ is a geometric factor describing the overlap of the laser and the receiver telescope as a function of range, $\beta_\pi(\lambda_0, R)$ is the atmospheric volumetric backscatter coefficient at range R for wavelength λ_0 , and is assumed to be homogenous over a slice of the atmosphere of thickness ΔR centered at R , and $\kappa(\lambda_0, R)$ is the volumetric extinction coefficient. The extinction coefficient $\kappa(\lambda_0, R)$ can be separated into 2 independent components for scattering and absorption as,

$$\kappa(\lambda_0, R) = \Sigma\alpha_i(\lambda_0, R) + \beta_{\theta \neq \pi}(\lambda_0, R) \quad (2)$$

Where $\beta_{\theta \neq \pi}(\lambda_0, R)$ represents all scatter from molecules or aerosols that is in other than the 180° backscatter direction, and $\Sigma\alpha(\lambda_0, R)$ represents absorption at wavelength λ_0 over the path to range R and the sum is over all absorbing constituents along the path. We can then rewrite Equation 1 as:

$$P_{rec}(\lambda_0, R) = P_L * C * \beta(\lambda_L, R) * \Delta R * e^{-2 \int_0^R \beta_{\theta \neq \pi}(\lambda_0, r) dr} * e^{-2 \int_0^R \Sigma_{i \neq 0} \alpha_i(\lambda_0, r) dr} * e^{-2 \int_0^R \alpha_{i=0}(\lambda_0, r) dr} \quad (3)$$

where C has been substituted for the factors that are dependent on the receiver and the last exponential is the absorption due to the molecule of interest. For a Differential Absorption Lidar (DIAL) measurement that uses on-line and off-line wavelengths very close together ($< \sim 0.1$ nm) $\beta_{\theta \neq \pi}(\lambda_0, R)$ can be considered constant over the wavelength range. Furthermore by appropriately selecting the wavelengths for a simultaneous coaxial measurement, differences in the absorption by all other molecules other than the molecule under investigation (second exponential in Equation 3) can also be made equal for the on and the off wavelengths. Note that this is not necessarily true for a pulsed lidar system from a high velocity spacecraft unless high repetition

rates are used, which in turn limits the unambiguous range. By taking the ratio of the two simultaneous measurements, and assuming the instrument is designed properly such that the receiver dependent differences at the two wavelengths are negligible, or constant and well calibrated, one arrives at the standard DIAL equation:

$$\frac{P_{rec}(\lambda_{off}, R)}{P_{rec}(\lambda_{on}, R)} = \frac{P_{Loff}}{P_{Lon}} e^{2\left(\int_0^R \alpha(\lambda_{on}, r) dr - \int_0^R \alpha(\lambda_{off}, r) dr\right)}$$

where, $e^{2\left(\int_0^R \alpha(\lambda_{on}, r) dr - \int_0^R \alpha(\lambda_{off}, r) dr\right)}$ is the round trip differential transmission between the on-line and off-line wavelengths to range R, from the Beer-Lambert law. If the transmitted power for both channels is monitored, $\frac{P_{Loff}}{P_{Lon}}$ is a known value and the measurement provides the differential transmission due to the molecule of interest. By taking the natural logarithm of the differential transmission, one is left with the differential absorption, $\left(\int_0^R \alpha(\lambda_{on}, r) dr - \int_0^R \alpha(\lambda_{off}, r) dr\right)$ which is related to the total column abundance of the gas between the sensor and range R by;

$$\int_0^R N(r) dr = \frac{1}{2} \int_0^R \frac{1}{\Delta\sigma(\lambda_{on}, \lambda_{off}, r)} dr * \left[\int_0^R \alpha(\lambda_{on}, r) dr - \int_0^R \alpha(\lambda_{off}, r) dr \right] \quad (5)$$

where $\Delta\sigma(\lambda_{on}, \lambda_{off}, R)$ is the differential cross section between λ_{on} and λ_{off} as a function of range to range R, determined through laboratory spectroscopy, and the quantity in brackets is the measured value from the lidar as described above. The 2 in the denominator is the result of the round trip path length from the transmitter to the scattering surface and back to the receiver. In reality $\Delta\sigma$ is a function of pressure, relative humidity and temperature in the atmospheric profile as well, and thus these quantities also need to be determined, but this is being neglected for the current discussion. For the IPDA measurement, R is taken to be the range to the scattering surface, $\beta(\lambda_L, R)$ is replaced with the surface reflectance $\rho(\lambda_L)$, and the integral is over the entire

column being measured. In the following sections we will describe the instrument developed by Exelis used to make the simultaneous IPDA measurement, and some results from LaRC's evaluation of the instrument.

3. Instrument Overview

Dobbs et al. [3] were among the first to apply the lock-in technique, often used in the laboratory environment for enhancing the sensitivity of signal recovery in the presence of noise, to laser remote sensing and to recognize that the IM-CW approach, has great potential in space-based remote sensing of planetary atmospheres [26][27]. MFLl utilizes the IPDA lidar technique using an IM-CW LAS for remote sensing of atmospheric CO₂ column amounts. Intensity modulation of a CW laser combined with an appropriate encoding algorithm allows the lock-in technique to be utilized to extract extremely weak signals in the presence of a large background signal with high SNR.

As described in the previous section, the MFLl laser transmitter uses two or more laser wavelengths (nominally, one "On" (on-line) the absorption line of the target gas and one "Off" (off-line) the line) to determine the column concentration of the atmospheric constituent of interest. In the simplest mode of operation for CO₂ measurements, the MFLl laser transmits CW laser light that is locked to the CO₂ on-line and off-line wavelengths. The intensity of laser light at each transmitted wavelength is modulated by a digitally generated, sinusoidal modulation signal. The frequency of the modulation signal on each channel is unique. The modulated signals in each channel are combined in an optical coupler and simultaneously amplified by a fiber amplifier. A reference for the output power signal at each wavelength is obtained by monitoring a portion of the resulting amplified signal. The amplified IM-CW signals are transmitted simultaneously to the surface. The backscattered returns from the surface as well as

intermediate clouds are collected with a telescope and focused into a multimode fiber. The background signal is filtered out using a narrow band optical filter and the signal is then converted to an AC coupled electrical signal using a sensitive optical detector and a Transimpedance Amplifier (TIA). This technique has strong advantages over other remote sensing techniques in that the background noise that is uncorrelated with the transmitted IM waveform is rejected with high fidelity from the desired signal during the lock-in process. However, the magnitude of the background light incident on the detector can limit the dynamic range of the desired signal. The reference and received signals are then analog band-pass filtered, digitally converted, and processed in the signal processing subsystem.

The intensity modulated backscattered signal is decoded using a digital lock-in to produce a narrow effective electronic bandpass filter, and as such, it allows a high SNR by reducing the sensitivity to broad bandwidth background and electronics noise sources. The fiber-laser-based architecture allows multiple IPDA wavelengths in and around the 1.57 μm wavelength region to be amplified and transmitted simultaneously. Since each IPDA wavelength is uniquely encoded, a single detector or detector array can be employed in the receiver. The returns at each wavelength can then be demodulated in software to produce the unique IPDA signals, which can be used to derive the CO_2 column measurements.

4. System Description

The MFLC contains a suite of IM-CW lidars that are all fundamentally similar in form and function. The generalized conceptual block diagram for a two-channel version of the MFLC is shown in Figure 1, and it includes a laser transmitter subsystem (shown in green), an input/output transfer optics subsystem (shown in orange), and a receiver subsystem (shown in blue). Key parameters for the latest implementation of the MFLC system are summarized in Table 1, and additional information about the MFLC system design can be found in [20][31][32].

The MFLC flight instrument was first built by Exelis in 2004 for a proof-of-concept demonstration, and it consists of mainly commercial, off-the-shelf components. Since then, the MFLC instrument has gone through many improvements and has participated in 10 major flight campaigns on 3 different aircraft in order for NASA Langley Research Center to evaluate the technology for the ASCENDS mission. The initial implementation of the IM-CW approach in MFLC used pure sine wave intensity modulation with each wavelength having a slightly different central frequency near 50 kHz. This implementation worked well for clear air cases, but for heavy aerosol loading or in the presence of thin clouds, it was not possible to distinguish returns from the atmospheric backscatter and those from the ground. Even fairly weak returns from intervening clouds/aerosols cause interference with the waveforms reflected from the surface when combined at the detector. To address the latter issue, in 2009 a unique approach for frequency balancing the system was implemented, which eliminated the interference effects but did not correct the partial path absorption effects. This patent-pending approach, which is referred to as tone-hopping, consists of using a series of modulation frequencies or tones that are cycled sequentially between the individual channels for at least one full cycle for each lock-in period. The result is that all channels have unique frequencies at any given time, but they all have the same frequency content over one complete lock-in period. This significantly improved the accuracy of the measurement due to interference effects, but it could not accurately address the partial path absorption effect introduced by the clouds/aerosols. To address this last effect, in 2010 the MFLC system bandwidth was increased, enabling the ability to intensity modulate the transmitted IPDA wavelengths with a time varying waveform that allowed the backscattered return from the surface and that from other intermediate scatter sources to be distinguished.

A block diagram of the MFL system used for IPDA measurements of CO₂ as flown in 2011 on the DC-8 aircraft is given in Figure 2. The O₂ component of MFL, which is required to determine the dry air surface pressure needed to convert the CO₂ number density column to an average CO₂ dry mixing ratio (XCO₂), is also shown in Figure 2. It operates on the same principles as the CO₂ instrument with the major difference being the use of a fiber Raman amplifier rather than an EDFA to amplify the combined O₂ on-line and off-line signals near 1262 nm before being transmitted. The 2011 flights were a first proof of concept of the O₂ channel and utilized a standard pin diode for the detector resulting in a much lower SNR than the CO₂ channel for the initial measurements. For this paper we are focusing on the more mature CO₂ component of MFL and a functional description of how the Exelis IM-CW measurement has been implemented. We plan to report additional details on the O₂ subsystem after a series of flights in early 2013 are completed in which a comparable detector system to the CO₂ receiver will be utilized for the O₂ channel. The MFL is composed of three main subsystems: the transmitter, the receiver, and the data system. Each of these subsystems is described in detail in the following sections.

4.1 Transmitter Subsystem

The transmitter subsystem is comprised of two laser systems: the laser transmitter associated with generating and transmitting the on-line and off-line CO₂ IPDA beams, and the laser altimeter transmitter providing the initial ranging from the aircraft to the surface.

4.1.1 LAS CO₂ transmitter

The IM-CW laser transmitter for CO₂ IPDA column measurements consists of: 1) a reference laser locked to a CO gas cell to continuously monitor the MFL laser wavelengths through a heterodyne process; 2) three Distributed Feedback (DFB) lasers controlled to ± 0.2 pm

as the signal lasers; 3) three Semiconductor Optical Amplifiers (SOA), each used to impart a unique intensity modulation to the signal wavelengths; 4) a polarization scrambler; 5) an EDFA, which amplifies the combined signal laser waveform to an average power of 5 W with a 0.004% fiber tap to monitor the outgoing power; and 6) a high quality fiber collimator used to decrease the transmitter divergence. All of the modulated laser wavelengths are transmitted simultaneously out of the single fiber collimator and thus have 100% spatial and temporal overlap. This eliminates sensitivity to highly varying surface reflectance as well as minimizing effects of atmospheric turbulence by making them common mode. The transmitter is all fiber-based and has no free-space optics; this results in a rugged design that does not have many of the alignment issues of a more complicated transmitter system typically employed for high-power lidar applications. The use of SOA's allows selection of relative amplitude of the three (on- and off-line) channels to compensate for atmospheric absorption effects and maintain detected signal levels. After combining the three modulated signals, a 90/10 splitter is used, with 90% seeding the EDFA and 10% being combined with the output of the reference laser that is locked to a CO absorption feature at a vacuum wavelength of 1571.14445 nm. The three lasers combined with the reference laser are sent to a high-speed InGaAs detector (EOTech ET-3500F). The beat frequency signal between the 3 wavelengths are monitored with an Anritsu MS2721A radio frequency (RF) spectrum analyzer. The precise wavelength of each laser is calculated, following repeated calibrations of the reference laser, from the beat frequency measurement and saved to disk.

4.1.2 Altimeter transmitter

The altimeter transmitter subsystem uses a 1596-nm fiber coupled DFB. The pseudo-random code is generated via a PXIe-6548, which digitally drives an electro-optic modulator attached to the DFB fiber output. The modulated signal is then sent to the EDFA, which

amplifies the signal to 5 W of average power and transmits it to the target via a co-aligned high-quality fiber collimator.

4.2 Receiver Subsystem

The reflected light from the target is collected by a single telescope and the CO₂ and O₂ signals are separated from the altimeter signal using an inline fiber based dichroic beam splitter, and then the CO₂ and O₂ signals are separated using a second inline fiber based dichroic. The CO₂ signal is sent through an optical bandpass filter to limit solar background and then focused onto a low excess noise 8x8 HgCdTe Avalanche Photodiode (APD) array with a TIA to convert the optical signal to an analog voltage signal. The signal is then AC coupled by passing through an analog bandpass filter, which also limits 1/f noise and aliasing. A high-resolution 16 bit, analog-to-digital converter is used to sample the analog waveform at 2 MHz, and the raw digital data are streamed directly to disk.

The fiber coupled altimeter signal is passed through an iris which is used to limit the signal reaching the detector to avoid saturation. The signal is then passed through a 3 nm optical bandpass interference filter, and focused onto the Photo Multiplier Tube (PMT) active area. The signal from the PMT is collected by an Ortec time-of-flight-digitizer and accumulated in 15 ns bins for 100 ms before being stored on the computer for processing.

The fact that the optical and electrical path are common mode for all of the signal wavelengths for the CO₂ IPDA measurement results in a significant reduction in sensitivity to instrument drift and noise from the atmosphere, target and sensor, which are combined into a common mode term that is removed when the signals are ratioed in the IPDA measurement.

4.3 Data Subsystem

The data system consists of two computers. The first computer is a custom, rack-mounted PC that is mainly used for hardware control and to collect and record ancillary data. It is also

used by the operator to monitor the instrument health and performance of MFL during flight. A National Instruments (NI) PXIe chassis is used to generate the digital representation of the tones that are then passed to the D/A converter and filtered before being passed to the modulation control electronics. It is also used for data acquisition and streaming the raw data to disk. There is also an NI PXIe-6682H GPS and timing card, which is used to provide GPS data and synchronize the clocks between computers. A small sub-portion of the data is processed in real-time and displayed for monitoring by the operator. In earlier versions, lower data acquisition rates (500 kHz) were used with the sinusoidal modulation, and the data was processed real time on a PXI chassis using a software-based digital lock-in. For the current system, four channels with 2-MHz sampling rates are being streamed directly to disk, and the majority of data processing is performed after the flight as described in the next section.

5. Signal Processing

IM-CW laser sensing has been extensively used in the laboratory for precise measurement of trace gas concentrations because of its high SNR and the relative simplicity of implementation [33]. The high S/N demonstrated by MFL is achieved in part by use of phase-sensitive detection implemented in a digital lock-in amplifier during signal processing.

5.1 Theory and Background

A digital lock-in amplifier uses a mathematical reference signal, a potentially noisy input digitally converted signal, and a phase-sensitive detector (PSD) to extract only that part of the output signal whose frequency and phase match the reference [27]. In this formulation, let the time varying signal be $V_{\text{sig}} \sin(\omega_{\text{sig}} * t + \theta_{\text{sig}})$ where V_{sig} is the signal amplitude, ω_{sig} is the signal frequency, and θ_{sig} is the signal's initial phase. To avoid confusing with the reference channel used to monitor the transmitted signal for the MFL we will refer to the mathematically

generated reference as the Local Oscillator (LO). The lock-in process multiplies the signal by the LO, $V_{LO} \sin(\omega_{LO} * t + \theta_{LO})$, through a point by point multiplication. To simplify the notation we will avoid the discrete representation for this discussion, but note that this is done in the digital domain. The output of the PSD is then simply the product of two sine waves,

$$\begin{aligned}
 V_{psd} &= \\
 V_{sig} * \sin(\omega_{sig} * t + \theta_{sig}) * V_{LO} * \sin(\omega_{LO} * t + \theta_{LO}) &= \\
 \frac{1}{2} * V_{sig} * V_{LO} * \cos([\omega_{sig} - \omega_{LO}] * t + \theta_{sig} - \theta_{LO}) & \\
 - V_{sig} * V_{LO} * \cos([\omega_{sig} + \omega_{LO}] * t + \theta_{sig} + \theta_{LO}). & \quad (6)
 \end{aligned}$$

Thus the PSD output is just two AC signals, one at the difference frequency ($\omega_{sig} - \omega_{LO}$) and the other at the sum frequency ($\omega_{sig} + \omega_{LO}$). If the PSD output is passed through a low pass filter, the AC signals are removed, and in the case where ω_{sig} equals ω_{LO} , the difference frequency component will be a DC signal proportional to the signal amplitude,

$$V_{psd} = \frac{1}{2} * V_{sig} * V_{LO} * \cos(\theta_{sig} - \theta_{LO}). \quad (7)$$

A lock-in with a single PSD is called a single-phase lock-in, and its output is $V_{sig} \cos(\theta)$ where $\theta = \theta_{sig} - \theta_{LO}$, which is sensitive to phase difference between the signal and the LO. This sensitivity can be eliminated with a second PSD that multiplies the signal with the LO shifted by 90° to produce

$$V_{psd2} = \frac{1}{2} * V_{sig} * V_{LO(90)} * \sin(\theta_{sig} - \theta_{LO(90)}). \quad (8)$$

The first output (V_{psd}) is referred to as the “in-phase” component (I) and the second output (V_{psd2}) as the “quadrature” component (Q). The phase dependency can be removed by computing the magnitude (R) of the signal as

$$R = (I^2 + Q^2)^{1/2} = V_{sig}. \quad (9)$$

The phase of the signal is

$$\theta = \text{atan}(Q/I), \quad (10)$$

and since the reference is a digitally generated function we have set V_{LO} and $V_{LO(90)} = 2$ to make the PSD output directly proportional to the actual voltage for the desired signal. Narrow band detection in the lock-in amplifier is key to achieving high S/N in the MFLM measurements. The noise at frequencies far from the reference are attenuated at the PSD output by the low pass filter, and only noise very close to the reference frequency will result in very low AC frequency outputs from the PSD and show up as noise in the received signals.

The discussion thus far has focused on sinusoidal modulations with unique fixed frequency. Consider the case where the frequency is ramped as a function of time. In this case we have a waveform given by $V_{sig} * \sin(\omega_{sig}(t) * t + \theta_{sig})$, where $\omega_{sig}(t)$ could be a linear or logarithmic changing frequency as a function of t and is a repeating function on a time cycle which corresponds to the desired unambiguous range. For example a linearly swept frequency may take the form

$$\omega_{sig}(t) = 2 * \pi * A * \left[\left(\frac{t}{a} - \text{floor} \left(\frac{t}{a} + 0.5 \right) \right) + 0.5 \right] \quad (11)$$

where “a” defines the sweep rate, or period, and “A” defines the sweep range.

In early experiments, MFLM transmitted on- and off-line output power with unique sinusoidal modulation frequencies ω_{on} and ω_{off} . In the clear air case, it is apparent that the signals necessary to obtain DIAL ratios can be detected directly using the PSD and knowledge of ω_{on} and ω_{off} . If intervening thin clouds or heavy aerosol layers are present the retrieval using simple sinusoidal signals will bias the retrieved CO_2 column measurements. Clearly, an approach is needed to discriminate between the ground-reflected signal and that returned by other atmospheric layers in the realistic case of thin clouds and heavy aerosol layers. Various frequency modulation schemes have been used in CW LAS systems to discriminate between

intermediate range scatter sources and hard targets [34-35]. We have investigated several approaches to providing this discrimination capability using pseudo-random noise modulation (PRN), discrete stepped intensity modulation (DSIM), and swept frequency modulation (SFM) schemes. We implemented the most promising technique that uses SFM with a linear monotonic sweep having a sequence length corresponding to ~ 15 km of the atmosphere. Lock-in, or autocorrelation, techniques are then used to retrieve the return signals from aerosols/clouds and the surface, separately. The ability to discriminate range for the MFLC IM-CW approach will ultimately lead to the ability to remove influences from thin clouds and aerosols.

5.2 Implementation

After the analog signals from the detector and TIA are passed through the analog bandpass filter and reach the processing system, there are three main operations: analog to digital conversion, lock-in or Fourier correlation, and calculation of the on/off signal ratio. A change from range-insensitive IM-CW techniques using unique but fixed modulation frequencies (with or without tone-hopping) to advanced range-discriminating IM-CW techniques using PRN, DSIM, or SFM has necessitated implementing advanced processing techniques that enable algorithms to discriminate ground from aerosol/cloud returns. Each of the processing steps is described in the following sections.

5.2.1 Analog to Digital Conversion

The current implementation of the MFLC uses a NI PXIe-6368 to simultaneously sample the reference and science detector analog signals in 16-bit samples at a rate of 2 MHz for each channel. The digital data are fetched from the PXIe card in chunks of 200,000 samples (0.1 s) and streamed to disk and memory. The raw data contain all of the simultaneous information contained in the multiple-wavelength backscattered signals and any noise not filtered out by the

AC coupling. Once the data sample blocks have been obtained, processing can be done in either of two forms – sample-by-sample lock-in or Fourier correlation.

5.2.2 Sample-by-Sample Lock-in

Sample-by-sample lock-in is modeled on the operation of a digital lock-in amplifier. The mathematical descriptions used to generate the output tones are retained and used to create both an in-phase (I) and quadrature (Q) LO of the same length. There are two LO's of 200,000 samples for every transmitted tone. These local oscillators are multiplied sample-by-sample against the incoming science and reference data, yielding 200,000 sample I and Q product pairs for each transmitted tone on each detector (science and reference) output. The mean of each of those I and Q products are then added in quadrature to produce a value representative of each tone's strength.

If the local oscillators are sine-waves, as is used in a normal lock-in amplifier, the above system provides a phase-invariant measure of each tone's amplitude within a narrow frequency bandpass. The width of that frequency bandpass is determined by the number of samples included in the mean. When the local oscillators use swept or stepped tones, the filtering is no longer phase-invariant. To measure the amplitude of a swept tone signal, the correlation function between the incoming data and LO are obtained. That is, correlation of the two data series should be performed. Since the frequency swept tones are fully repeated after each integration length (or lock-in period) the correlation can be calculated through circulating the LO, or the instrument signal, through the 200,000 possible offsets. Individual steps in this circular correlation represent their corresponding time-delays, and thus the range based on time of flight. Altimeter readings have been used to set this rotation (or phase shift) in real-time to obtain in flight results for the operators to evaluate instrument performance, and to limit the post processing computing requirements. However, this technique limits one to examining the results

only at the phase offset of the strongest returns for the altimeter, which may not correspond to the range of interest.

During the development of the MFLL, three main types of IM-CW tones have been used. Prior to 2009, each output wavelength was given a unique and constant sinusoidal frequency modulation. From 2009 through early 2011, the IPDA wavelengths would trade these tones (tone-hopping) every 1000 samples. This frequency modulation was done to balance the effects of multipath superposition and electrical frequency response variations across all channels, with the side effect of adding noticeable but negligible phase dependence. With the instrument's 2011 sampling-rate upgrade to 2 MHz and the implementation of the new swept waveforms, phase matching the local oscillator and incoming data became a vital concern.

Due to some technical issues during a few flight segments with an older REACH telemetry output card that was used to generate the PN code, there were some gaps in altimeter records. Because of this, the initial 2011 post-processing entailed computing the lock-in values for a range of local oscillator phase shifts about the assumed altitude from GPS data. The strongest signal from the center of the phase window was assumed to be coming from the ground. When the strongest return was found to be at the edge of the phase window, it was assumed to be the result of a large reflection from a cloud and filtered out.

The processing advance to wanting to measure the returns from both the cloud(s)/aerosols and the ground. To accomplish this one can compute returns across the whole column by performing the lock-in for every rotation of the local-oscillator. This approach is computationally intensive, and the process further progressed to implementation of a correlation by Fourier transform.

5.2.3 Fourier Transform Correlation

Correlation by Fourier transform begins by pre-computing the complex conjugate of the Fourier transform of the LO's. Those conjugate LO's are then multiplied by the Fourier transform of our incoming data, which includes the 200,000 point samples from the science and reference detectors. The resulting 200,000 products are then inverse Fourier transformed and the resulting I and Q samples are then added in quadrature. This technique results in a curve for each tone that is representative of the waveform amplitude at a given phase delay which is related to the amplitude received from each range bin, where the range bin distance is defined by the sampling rate. Examples of these waveforms and fitting methods to improve the range resolution beyond the sampling rate inherent range bins are presented in Section 6.

5.2.4 IPDA Differential Transmission or Grand Ratio

For fixed frequency outputs, the maximum peaks of the Fourier curves are equivalent to the resulting value of the lock-in calculation. Having found separate values for both off-line and on-line data sets for each given tone, one can determine the IPDA differential transmission by taking the ratio of the normalized on-line to off-line returns, i.e., $(\text{on-line_science}/\text{on-line_reference})/(\text{off-line_science}/\text{off-line_reference})$, which we call the Grand Ratio. As described in Section 2 the Grand Ratio is the measurement which can be used with knowledge of the differential cross section to retrieve the total column number density. This can then be used, as described in Section 6, along with the measured temperature, pressure and relative humidity, to derive the XCO₂ product and to compare with the independent in-situ measured values.

5.2.5 Filtering of Cloud Returns

With the capability to use ranging waveforms, one isn't limited to determining only the maximum peak of the Fourier curves. The maximum peak represents the maximum

backscattered return, but that return may be from clouds or other intermediate backscatter sources rather than from the desired column to the surface. The Fourier curves are like the return from a pulse-lidar that has been convolved with a point-spread function that happens to be the autocorrelation of the generated tones. Further, one can think of the curve as being made of the linear combination of that autocorrelation function at all delays through the atmosphere. At computational expense, the returns from backscatter sources at all ranges/altitudes can be determined, and ultimately one should be able to remove the contributions from all ranges other than the range of interest. We are in the process of exploring more advanced retrieval algorithms that are less computationally demanding in order to determine and isolate the desired range-dependent scattering profiles, and these will be discussed in a later paper.

6. MFLL Flight Test Campaigns

Ten major flight test campaigns of the MFLL have been conducted since May 2005 to evaluate its capability to make remote CO₂ column measurements. Figure 3 shows the installation of MFLL on different aircraft and a list of the flight test campaigns; when and where they were conducted; how many flights were in each campaign; what aircraft was used; whether the flights were over land and/or water; what the solar background conditions were; and additional comments about the campaigns. The flight campaigns were designed to permit MFLL testing under a number of measurement conditions. Most of the campaigns, with the exception of one flight during the 2008 Newport News campaign and one in the 2011 Palmdale campaign, were conducted in rural/remote locations to try to avoid spatially variable CO₂ conditions associated with power plant and urban plumes. The flight tracks for MFLL evaluations were typically orientated along the low-level wind direction as defined by the 800 hPa wind vectors. This ensures that we would be remotely measuring a reasonably homogeneous CO₂ condition

along the flight leg. MFLL flight legs of 50-100 km in length were flown repeatedly at one altitude and then at many different altitudes up to the high altitude limit of the aircraft. Typical altitude ranges were from about 3 km to about 8 km for the Lear-25 and UC-12 flights, and from about 3 km to above 12 km for the DC-8 flights. This strategy was used to determine the consistency of the remote CO₂ measurements and their correlation with altitude. In addition, for comparison with the MFLL remote CO₂ column measurements, *in situ* CO₂ profiles were obtained during each flight near the center of the flight legs from as low an altitude as possible to the highest flight test altitude on that day. The CO₂ and meteorological *in situ* measurements are from instruments onboard the aircraft and from collocated radiosonde measurements as discussed in the next section. Flights were conducted both during the day and at night, over a wide range of surface conditions (land and water), and in clear and scattered-cloud conditions. As previously noted, prior to 2011 the MFLL was operated in the 50 kHz (nominal) fixed-frequency mode with or without tone-hopping, and in the 2011 DC-8 flight test campaign, the MFLL was operated in the swept-frequency mode.

6.1 MFLL Surface Reflectance and CO₂ Measurement Precision Results

Early MFLL flights on the Lear-25 provided the first measurements of the variability of the surface reflectance at 1.57 μm and the relative precision of the remote CO₂ column measurements. Examples of these measurements can be seen in Figure 4 on a water-to-land flight leg made on 22 October 2007 near the VA Eastern Shore. This figure shows the simultaneous on-line and off-line MFLL return signals with 1 s averaging from an altitude of 3.3 km and the calculated CO₂ column optical depth along the flight track shown at the top. On that day the reflection from the water was a factor of 3 to 4 less than from land, and the land surface reflectance also varied by a factor of 2.5 along the track due to abrupt changes in the surface

types, e.g., transitions between different agricultural land/vegetation surfaces and stands of trees, etc. Because the MFL signals were obtained simultaneously, the spatial correlation in the signal variations due to surface reflectance changes is identical in all signals. Even the reflectance change associated with the small peninsula of land protruding into the bay observed at 11.062 hrs shows up identically in both signal channels. The high correlation in the surface reflectance variations between the on- and off-line channels allow them to be eliminated when the ratios are taken and the CO₂ optical depths (OD) are calculated as shown in the figure. Also, note that there was no change in the average CO₂ OD across the water-to-land transition. On these early flights the average CO₂ OD SNR for a 10-s average, which corresponds to about 1 km, was found to be 291 over water and 396 over land. These SNR values correspond to a CO₂ mixing ratio measurement precision of about 1.3 and 0.97 ppmv, respectively. Note that for general reference we frequently relate the relative precision in the CO₂ column optical depths ($\sigma_{OD} = 1/SNR_{OD}$) to the relative precision in the CO₂ column mixing ratios (σ_{XCO_2}) by simply multiplying the average background value of XCO₂ (384 ppmv in this case) by σ_{OD} . The higher CO₂ OD SNR (lower CO₂ OD and XCO₂ uncertainties) over land compared to water is entirely due to the higher surface reflectance and higher return signals over land. As the following results will show, the MFL CO₂ measurement precision improved considerably after transitioning to the more thermally controlled cabin environment associated with the UC-12 aircraft and transitioning from fixed frequency sine wave modulation to the rolling tone modulation.

A comprehensive multiple-aircraft flight test program with the MFL on the UC-12 was conducted over Oklahoma and Virginia in July and August 2009. Figure 5 shows an example of the MFL-derived surface reflectance and average CO₂ column variations along a flight leg over

the Department of Energy's (DOE) Atmospheric Radiation Measurement (ARM) Central Facility (CF) in Lamont, Oklahoma on 31 July. A 1 s average (~100 m) was used for the surface reflectance measurements and the average CO₂ OD column measurements, which are expressed in terms of XCO₂ units. As seen in Figure 5, the surface reflectance signal determined from the off-line channel varies by more than a factor of 2 over short distances along the leg, but the variations in the derived XCO₂ are generally within ± 1.5 ppmv of the average value of 378 ppmv. The average MFLX XCO₂ SNR for 1-s horizontal averages along the leg was found to be 760, which is an effective XCO₂ measurement precision of 0.60 ppmv, and for a 10 s average the SNR was found to be 2002 for a precision of 0.20 ppmv. On a subsequent flight over the Chesapeake Bay from 4.6 km on 12 August, the 10-s XCO₂ SNR was found to be 1300 for a precision of 0.30 ppmv.

The MFLX instrument was flown during the first DC-8 ASCENDS Test Flight Campaign conducted from 8 to 18 July 2010 from the NASA Dryden Flight Research Facility in Palmdale, California. Flights were conducted during clear, mostly cloud-free, atmospheric conditions over a wide range of surface types, including the satellite radiometric calibration location of Railroad Valley (RRV), Nevada; the desert region near Needles, California; the vegetated farmland of the Central Valley of California; the farmland around the DOE/ARM CF; and the eastern Pacific Ocean, just off Baja. Table 2 shows the average reflectance measured for each of these surface types as derived from the off-line backscattered signals, which were scaled to a common 7 km altitude above the surface and then scaled to a RRV surface reflectance of 0.14 sr⁻¹ at 1.57 μ m [36] (Note that this is only a relative scaling, which does not attempt to include an additional factor for the laser backscatter enhancement in the 180° backscatter direction). The playa reflectance of RRV was 0.176 sr⁻¹. The average vegetation reflectance of the Central Valley,

CA, and near Lamont, OK, was found to be 0.12 sr^{-1} , which is similar but lower than RRV. The ocean reflectance on the one flight in 2010 was underestimated due to a system misalignment issue on that flight, but previous Chesapeake Bay measurements from the 2009 flight campaign showed higher reflectance. The ocean reflectance is driven by the mean surface wind condition [37], and the ocean reflectance can vary from high values of 0.1 sr^{-1} at very low wind speeds ($<1 \text{ m/s}$) to low values of $<0.03 \text{ sr}^{-1}$ at wind speeds greater than 10 m/s .

The average SNR of the MFL CO₂ column measurements was estimated on flights over each of the surfaces indicated in Table 2. Estimates of 1-s and 10-s SNR values were made from the 10 Hz OD measurements in each 1 s and 10 s interval (using the relationship $\sigma/(N-1)^{1/2}$, where σ is the standard deviation, and N are the number of data points) along the entire flight leg. This approach helps to eliminate the spatial variations in CO₂ OD on SNR determination from OD variations along the leg that are due to real larger-scale CO₂ column changes. An average is taken of all the SNR estimates in each interval over the flight leg, and that value is shown in Table 2 along with an estimate of the equivalent standard deviation in terms of XCO₂. The highest 1 s SNR's (>600) were found, as expected, over the highest reflectance desert surfaces, and this produced a CO₂ measurement sensitivity of better than 0.6 ppmv . The SNR decreased to about 550 over vegetated surfaces with a measurement sensitivity of about 0.7 ppmv . With a 10 s averaging interval, all of the land SNR values increased to >1300 for the desert surfaces and to nearly that level for the vegetated surfaces. This increase resulted in CO₂ measurement sensitivities of better than 0.3 ppmv for all of the land surfaces. As found on previous flight campaigns, the 1 s SNR over water was significantly reduced from the over land measurements, but the 10 s SNR over water was found to be about comparable to the 1 s SNR over land.

6.2 Evaluation of MFL CO₂ Column Measurement Accuracy

6.2.1 Methodology for Determining *In Situ*-derived CO₂ Column ODs

To derive the true CO₂ optical depth (OD) to compare with the MFL remotely-measured CO₂ OD requires knowledge of the vertical profile of XCO₂, the profile of meteorological parameters, the path length from the aircraft to the surface, and the off-nadir pointing of the laser beam. As mentioned previously, test flights were designed to facilitate the comparison of MFL remote ODs with *in situ*-derived ODs by including multiple overpasses of a comparison point and data obtained on a spiral at the comparison point. During the aircraft spiral, high-quality *in situ* measurements of CO₂ [38][39], temperature (T), pressure (P), and relative humidity (RH) were obtained from onboard instruments. In addition, *in situ* meteorological measurements from collocated radiosonde launches were obtained. Also on board the aircraft, laser altimeter measurements provided information on the range to the surface or cloud, a GPS provided aircraft altitude and location, and the aircraft navigation system provided attitude information. The information from all of these sources was used to derive the true two-way CO₂ OD ($\Delta\tau$) from the equation:

$$\Delta\tau = 2 \int_{z=b}^{z=t} \Delta\sigma(\lambda_{on}, \lambda_{off}, T, P, z) \cdot \eta(T, P, RH, z) \cdot \delta z \quad (12)$$

where α is the differential absorption cross section profile, η is the *in situ* dry CO₂ number density profile, and δz is the vertical bin size. Profiles of T and P are used in both the CO₂ absorption cross section and CO₂ number density calculations, and RH is used in the calculation of the dry CO₂ number density. The integration is performed over the vertical distance from the

aircraft altitude (t) to the scattering surface (b). When data were taken during an aircraft turn the pitch and roll information were used to convert the MFLL measurements to an equivalent nadir measurement. The *in situ*-derived ODs were also calculated for the same vertical range as determined from the attitude corrected path length.

The Voigt approximation of the CO₂ absorption cross section was used in these calculations, which requires input for the position of the absorption line, the molecular line strength, air broadened half width, temperature dependence coefficient, and lower-level energy E. In our calculations we used the HITRAN 2008 database [40] and the measurements of the line parameters by Devi et al. [41]. We included absorption from neighboring CO₂ lines and the contribution from other gases near the line center.

Comparisons of MFLL and *in situ*-derived ODs were typically limited to a region within 10 km of the comparison location, and when multiple *in situ* spirals were conducted during a flight, we used the spiral data closest in time to the MFLL overpass. The MFLL OD measurements were averaged over the time we were close to the spiral location and that value was compared to the *in situ-derived* OD. The GPS aircraft altitude, range to the surface from the altimeter, and the Global Land One-kilometer Base Elevation (GLOBE) database [42] were used to eliminate cloud-obstructed data from the comparisons. Comparisons between the MFLL and *in situ* measurements were reported as ODs and as equivalent XCO₂ values. The conversion to equivalent XCO₂ was accomplished by simply dividing the ODs by the *in situ*-derived OD for the equivalent of a constant 1 ppmv of CO₂. The only adjustment to the MFLL CO₂ OD measurements for the 2011 campaign data was to account for differences between the PN altimeter range and the lower spatial resolution of the digitized modulation signals. An empirical relationship was established between these ranges and the measured OD on one flight leg on 9

August 2011, which exhibited a wide span of range differences over a short flight distance, and it was applied uniformly to all MFL CO₂ OD measurements on all other flight legs throughout the campaign. It should be noted that this correction was small and upgrading the MFL to higher digitization rates in the future should eliminate the need for this type of correction.

6.2.2 Most Recent Comparisons of MFL and *in situ* CO₂ Measurements

During the 2011 DC-8 flight test campaign, the MFL system was modified to operate in a swept-frequency mode to provide the potential for range discrimination in the CO₂ measurements. This modification will eventually eliminate the need for the separate altimeter in the MFL system, as briefly discussed in the next section. Example comparisons of MFL CO₂ OD measurements with *in-situ*-derived (modeled) ODs are presented in Figure 6 for two very different conditions. The top example shows the MFL CO₂ OD measurements on a constant altitude flight leg over the Central Valley, CA in comparison to modeled ODs derived from *in situ* CO₂ data obtained on a DC-8 spiral at the center of the leg and radiosonde data obtained within about 1 hour of the overflight. The small variations in the modeled OD across the flight leg were due to small changes in the range from the aircraft to the surface. The resulting average difference between the measured and modeled ODs on the Central Valley flight leg was found to be -0.28% or the equivalent of ~1.1 ppmv. The second example at the bottom of Figure 6 shows the OD comparison while transiting across the Rocky Mountains. The *in situ* data (spiral and radiosonde) came from RRV, and the variation in ODs across the mountains is almost entirely due to surface elevation changes as the aircraft was at a constant altitude. The measured and modeled OD comparison showed a high level of agreement ($\Delta OD = -0.44\%$ or ~1.7 ppmv) even

when one expects that some change in CO₂ across the mountains that could not be captured in the modeled OD due to the lack of *in situ* data was present.

A comprehensive set of comparisons of MFL measured versus modeled CO₂ ODs was conducted during the 2011 DC-8 flight test campaign, and the results are presented in Figure 7. Six flights during this campaign were used in these comparisons, and the two flights that were not included had an extremely high fraction of optically-thick cloud that precluded quantitative comparisons. When the cloud fraction was less than about 50% below the aircraft on a flight leg, cloud detection and filtering of data was conducted to limit all comparisons to cloud-free conditions. A total of 38 comparisons are shown in the figure covering a range from the aircraft to the surface of 3 to 13 km. No range-dependent trend in the CO₂ differences was found, and the average difference (measured minus modeled) of all the comparisons (shown by the blue line) was found to be -0.65 ppmv with a standard deviation of 1.7 ppmv. These results are very similar to those obtained during the 2009 and 2010 MFL flight test campaigns [6][43].

While this current set of CO₂ comparisons demonstrates an unprecedented absolute accuracy of the MFL remote measurements of CO₂ ODs, we believe that this can be even further improved by using the extensive information content in the swept-frequency modulation technique being employed now in the MFL. Potential advantages include: the ability to do ranging directly with the MFL off-line signal, thus eliminating the need for a separate altimeter and the need to use a measurement calibration between the altimeter and the CO₂ signals; and the ability to detect and range to intermediate clouds along the line-of-sight and to use this information to remove the influence of optically-thin intermediate clouds on the CO₂ OD column measurement. A detailed review of these new areas of research, are beyond the scope of this current paper, but they will be discussed in a future publication and briefly touched on in the following section.

6.3 Range Measurements

As discussed in Section 5, a cross correlation of the LO signal and science signals can be used to determine the temporal delay between the LO and the signals (Science and Reference).

The autocorrelation function for a swept frequency system is

$$|P(t)| = C \left| \frac{\sin\left[\pi \Delta f t \left(1 - \frac{|t|}{\tau}\right)\right]}{2\pi \Delta f t \left(1 - \frac{|t|}{\tau}\right)} \right|, 0 < t < \tau \quad (13)$$

where C is the peak amplitude of the correlation, τ is the time required to complete one frequency sweep, and Δf is the frequency range of the sweep [44, 45]. Equation 13 can be modified for a cross correlation by introducing a term for the phase delay between the LO and science signals as in

$$|P(t)| = C \left| \frac{\sin\left[\frac{\pi \Delta f}{a} (t-b) \left(1 - \frac{|t-b|}{\tau}\right)\right]}{2\pi \Delta f (t-b) \left(1 - \frac{|t-b|}{\tau}\right)} \right| \quad (14)$$

where b is the phase delay, C is the peak amplitude of the cross correlation, and a adjusts the width of the correlation peak to account for environmental interactions (such as elevation changes or distributed returns due to clouds). To ease the computation burden of the parameter fit, Equation 14 can be approximated by a normalized sinc function as in

$$|P(t)| = C \left| \frac{\sin\left[\frac{\pi (t-b)}{a'}\right]}{\frac{\pi (t-b)}{a'}} \right| \quad (15),$$

where a and a' are related by a scalar, which is not important for this current discussion.

For a swept frequency system, the inherent range resolution (RR) and sample resolution (SR) is $RR = c / (2 * BW)$ and $SR = c / (2 * DAR)$ where c is the speed of light, BW is the sweep bandwidth, and DAR is the data acquisition rate. The maximum unambiguous range (MUR) is $MUR = c * \text{tausamples} / (2 * SR)$ where tausamples is the number of samples in the time required for one frequency sweep. For current MFL implementation (limited by $DAR = 2 \text{ MHz}$ and $\Delta f = 500 \text{ KHz}$) yields a range resolution of $RR = 300 \text{ m}$, a sample resolution of $SR = 75 \text{ m}$, with

MUR chosen to be 15 kilometers (tausamples = 200 samples). The SR is the raw resolution which one can determine the range to a single target, while the RR is a measure of the ability to distinguish between two closely spaced scattering sources and is essentially the full-width at half-maximum of the correlation function. Both SR and RR can be improved on by fitting and advanced signal processing.

By fitting Equation 14 or 15 to the output of the lock-in processor, significantly higher range accuracies can be achieved as illustrated in Figure 8. An example of range measurements using the swept frequency modulation technique with the empirical correction to the CO₂ + 50 pm off-line channel data are shown in Figure 9 that are compared with range measurements with the on-board altimeter. Ranging precisions to within about 3 m have been achieved.

We are in the process of improving this ranging capability. Higher ranging precision has been demonstrated from our recent ground tests with fixed target at LaRC during July-August 2012. The algorithm development and retrieval of range will be the subject of a follow on paper and initial results are presented here for completeness. Higher sampling rates would improve the fit (at the cost of computational complexity and data volume) and specifically improve the amplitude recovery, negating the need for the small correction mentioned in the previous section. We are currently working on improving the processing algorithm to directly correct for the small, repeatable deviation as the true range deviates from integer multiples of 75 m, versus using the empirical correction described in the previous section, until we can upgrade the A/D to a higher rate system and eliminate the need for this correction.

The ability to discriminate range for the MFLL IM-CW approach will ultimately lead to the ability to remove influences from thin clouds and aerosols in addition to eliminating the need to fly a separate altimeter. We conclude this brief discussion of the new range discrimination

technique for the IM-CW approach, with an example of two series of range measurements over regions of clouds with strong and weak return signals which are illustrated in Figure 10. Other potential variations of the frequency and waveform, beyond the linear frequency swept waveform, are also being investigated for improving ranging and processing capability.

7.0 Conclusions

Exelis and NASA Langley Research Center have exerted extensive effort and resources in order to develop, demonstrate, and validate the MFL instrument. This effort has allowed us to significantly mature the measurement technique and demonstrate high-precision column CO₂ measurements and demonstrate the potential to meet the needs of the future ASCENDS space mission. The MFL was built mainly from commercial off the shelf components and operated in a broad range of conditions over several years. We have demonstrated the measurement using an appropriately temperature- and RH-insensitive CO₂ absorption line at 1.571112 μm. This line was selected, in part, to take advantage of relatively mature fiber laser and efficient detector technologies. The transmitter is a low peak power all fiber-based CW laser and has no free space optics, which results in a rugged design that does not have many of the alignment, or high peak power, issues of more complicated transmitter systems typically employed for high-power pulsed lidar applications. MFL has proven to be robust enough to operate on 3 different aircraft during 10 major campaigns with more than 70 flight sorties and more than 1000 hours of ground testing, with the same laser and detector. CW modulation and digital ‘lock-in’ signal processing extract only that part of the output signal where the frequency and phase match the reference, thus enhancing the signal-to-noise ratio of the detected signal. Different modulation techniques have been tested/employed to obtain precise ranging capability to the surface, and further work is ongoing. Very high precision (<0.3%) CO₂ ODs have been demonstrated from a number of field

experiments over a variety of land surfaces over short (~ 100 m) spatial and temporal (1-s) scales. Absolute comparisons of remotely sensed and *in situ* CO₂ measurements showed agreement on average to better than 0.65 ppmv of CO₂ with a standard deviation of the differences to better than 2 ppmv. Ranging capability to intermediate scattering sources and to the surface has been demonstrated with the ability to discriminate between them. These developments support a clear path toward the successful development of a space-based CO₂ active remote sensing capability. Current and future work is directed at continuing to mature the technology and demonstrating the ability to scale this technology the ASCENDS mission.

We would like to thank Berrien Moore III for his leadership in advocating for the space mission (ASCENDS), Scott Zaccheo for assistance in selecting appropriate laser lines for our measurements and data analysis support, Stephanie Vay for leading the *in situ* CO₂ measurement team on the DC-8 campaigns, Christopher Thornton for radiosonde launches and logistics on the DC-8 campaigns, Mike Dobbs for the initial development and early evaluation of the MFL instrument, Marta Fenn for assistance in the MFL data processing and analysis, Amin Nehrir for comments on the draft manuscript, and Frank Cutler for the DC-8 project management and coordination of all DC-8 ground and flight activities. We would also like to thank the crews of the Uc-12 and Lear-25 along with the countless others that have participated in this several year effort.

References

1. Intergovernmental Panel on Climate Change, “Climate Change 2007: The physical Science Basis, Contribution of Working Group I to the Fourth Assessment Report of the Intergovernmental Panel on Climate Change”, Solomon, S., D. Qin, M. Manning, Z. Chen, M. Marquis, K. B. Averyt, M. Tignow, and H. L. Miller, Eds., Cambridge University Press, Cambridge, UK, 996 pp (2007).
2. National Research Council, “Earth Science and Applications from Space: National Imperatives for the Next Decade and Beyond”, the National Academies Press, Washington, D.C. (2007).
3. Dobbs, M. E., J. Dobler, M. Braun, D. McGregor, J. Overbeck, B. Moore III, E. V. Browell, and T. Zaccheo, “A Modulated CW Fiber Laser-Lidar Suite for the ASCENDS Mission”, Proc. 24th International Laser Radar Conference, Boulder, CO, 24-29 July 2008.
4. Dobler, J., et al., “Advancements in a multifunctional fiber laser lidar for measuring atmospheric CO₂ and O₂”, Proceedings, 16th Symposium on Meteorological Observation and Instrumentation, 92nd AMS Annual Meeting, New Orleans, LA, 22-26 January 2012.
5. Browell, E. V., M. E. Dobbs, J. Dobler, S. Kooi, Yonghoon Choi, F. W. Harrison, Berrien Moore III, and T. S. Zaccheo, “Airborne demonstration of 1.57-micron laser absorption spectrometer for atmospheric CO₂ measurements”, Proceedings, 24th International Laser Radar Conference, Boulder, CO, 23-24 June 2008.
6. Browell, E. V., et al., “Airborne validation of laser remote measurements of atmospheric carbon dioxide”, Proceedings, 25th International Laser Radar Conference, St. Petersburg, Russia, 5-9 July 2010.

7. R. Agishev, B. Gross, F. Moshary, A. Gilerson and S. Ahmed, “Atmospheric CW-FM-LD-RR lidar for trace-constituent detection: a concept development”, *Applied Physics B: Lasers and Optics*, 81, 695-703 (2005).
8. Browell, E. V., et al., “Airborne laser CO₂ column measurements: Evaluation of precision and accuracy under wide range of conditions”, Presented at Fall AGU Meeting, San Francisco, CA, 5-9 December 2011.
9. Browell, E. V., et al., “Airborne validation of laser CO₂ and O₂ column measurements”, *Proceedings, 16th Symposium on Meteorological Observation and Instrumentation, 92nd AMS Annual Meeting, New Orleans, LA, 22-26 January 2012.*
10. C. E. Miller, D. Crisp, P. L. DeCola, S. C. Olsen, J. T. Randerson, A. M. Michalak, A. Alkhaled, P. Rayner, D. J. Jacob, P. Suntharalingam, D. B. A. Jones, A. S. Denning, M. E. Nicholls, S. C. Doney, S. Pawson, H. Boesch, B. J. Connor, I. Y. Fung, D. O’Brien, R. J. Salawitch, S. P. Sander, B. Sen, P. Tans, G. C. Toon, P. O. Wennberg, S. C. Wofsy, Y. L. Yung, and R. M. Law, “Precision requirements for space-based XCO₂ data,” *J. Geophys. Res.* 112 D10314, doi: 10.1029/2006JD007659 (2007).
11. Crisp, D., R.M.Atlas, F.M.Breon, L.R.Brown, J.P.Burrows, P.Ciais, B.J.Connor,S.C.Doney, I.Y.Fung, D.J.Jacob, C.E.Miller, D.O’Brien, S.Pawson,J.T.Randerson, P.Rayner, R.J.Salawitch, S.P.Sander, B.Sen, G.L.Stephens,P.P.Tans, G.C.Toon, P.O.Wennberg, S.C.Wofsy, Y.L.Yung, Z.Kuang, B.Chudasama, G.Sprague, B.Weiss, R.Pollock, D. Kenyon, and S. Schroll, “The Orbiting Carbon Observatory (OCO) Mission.” *Adv. Space Res.*, 34, 700–709 (2004).

12. D. O'Brien, and P. J. Rayner, "Global observations of the carbon budget: 2. CO₂ column from differential absorption of reflected sunlight in the 1.61 μm band of CO₂", *J. Geophys. Res.*, 107, 4354, doi:10.1029/2001JD000617 (2002).
13. R. Measures, "*Laser Remote Sensing: Fundamentals and Applications*" (Krieger Publishing Company, New York, 1992).
14. G. J. Koch, J. Y. Beyon, F. Gibert, B. W. Barnes, S. Ismail, M. Petros, P. J. Petzar, J. Yu, E. A. Modlin, K. J. Davis, and U. N. Singh, "Side-line tunable laser transmitter for differential absorption lidar measurements of CO₂: Design and application to atmospheric measurements", *Appl. Opt.* 47, 944–956 (2008).
15. Barkley, M.P., P.S. Monks, R. J. Engelen, "Comparison of SCIAMACHY and AIRS CO₂ measurements over North America during the summer and autumn of 2003," *Geophys. Res. Lett.*, 33, L20805, doi:10.1029/2006GL026807 (2006).
16. T. Yokota, H. Oguma, I. Morino, A. Higurashi, T. Aoki, and coauthors, "Test measurements by a BBM of the nadir-looking SWIR FTS aboard GOSAT to monitor CO₂ column density from space", *Proc. SPIE.* **5652**, 182, doi:10.1117/12.578497 (2004).
17. M. Chahine, C. Barnet, E. Olsen, L. Chen, and E. Maddy, "On the determination of atmospheric minor gases by the method of vanishing partial derivatives with application to CO₂ ." *Geophys. Res. Lett.*, **32**, L22803, 10.1029/2005GL024165 (2005).
18. H. Bosch, et al., "Space-based near-infrared CO₂ measurements: Testing the Orbiting Carbon Observatory retrieval algorithm and validation concept using SCIAMACHY observations over Park Falls, Wisconsin", *J. Geophys. Res.*, 111, D23302, doi:10.1029/2006JD007080 (2006).

19. R. Menzies, and D.M. Tratt, "Differential laser absorption spectrometry for global profiling of tropospheric carbon dioxide: selection of optimum sounding frequencies for high precision measurements," *Appl. Opt.*, 42, 6569-6577 (2003).
20. M. Dobbs, W. Sharp, E.V. Browell, T. S. Zaccheo, and B. Moore III, "A sinusoidal modulated CW integrated path differential absorption lidar for mapping sources and sinks of carbon dioxide from space," 14th Coherent Laser Radar Conference, Snowmass, CO, 8-13 July 2007.
21. G. Ehret, C. Kiemle, M. Wirth, A. Amediek, A. Fix, and S. Houweling, "Spaceborne remote sensing of CO₂, CH₄, and N₂O by integrated path differential absorption lidar: A sensitivity analysis," *Appl. Phys. B*, 90, 593-608;doi:10.1007/s00340-007-2892-3 (2008).
22. A. Amediek, A. Fix, M. Wirth, and G. Ehret, "Development of an OPO system at 1:57 μm for integrated path DIAL measurement of atmospheric carbon dioxide," *Appl. Phys. B* 92, 295–302 (2008).
23. S. Kameyama, M. Imaki, Y. Hirano, S. Ueno, D. Sakaizawa, S. Kawakami, and M. Nakajima, "Development of 1:6 μm continuous-wave modulation hard-target differential absorption lidar system for CO₂ sensing", *Opt. Lett.* 34, 1513–1515 (2009).
24. J. B. Abshire, H. Riris, G. R. Allan, C. J. Weaver, J. Mao, X. Sun, W. E. Hasselbrack, S. R. Kawa, and S. Biraud, "Pulsed airborne lidar measurements of atmospheric CO₂ column absorption," *Tellus B*, 62, 770–783 (2010).
25. S. Kameyama, M. Imaki, Y. Hirano, S. Ueno, S. Kawakami, D. Sakaizawa, T. Kimura, and M. Nakajima, "Feasibility study on 1:6 μm continuous-wave modulation laser absorption spectrometer system for measurement of global CO₂ concentration from a satellite", *Appl. Opt.*, 50, 2055-2068 (2011).

26. J. Pruitt et al., "High-speed CW lidar retrieval using spectral lock-in algorithm", *Proceeding of the SPIE*, vol. 5154, p 138 (2003).
27. M. Dobbs, M., J. Pruitt, D., Gregory, & W. Sharp, W., "Matched Filter Enhanced Fiber-based Lidar for Earth, Weather and Exploration", *AGU Fall Meeting*, A1194, San Francisco, CA, 11-15 December 2006.
28. Browell, E. V., et al., "First Airborne Laser Remote Measurements of Atmospheric CO₂ for Future Active Sensing of CO₂ from Space", *Proceedings of the 8th International Carbon Dioxide Conference*, Jena, Germany, 13-18 September 2009a.
29. E. Browell, M. E. Dobbs, J. Dobler, S. Kooi, Y. Choi, F. W. Harrison, B. Moore III, and T. S. Zaccheo, "First airborne laser remote measurements of atmospheric CO₂ for future active sensing of CO₂ from space", *Proceedings of the 8th International Carbon Dioxide Conference*, Jena, Germany, 13-18 September 2009b.
30. E. Browell, , M. E. Dobbs, J. Dobler, S. Kooi, Y. Choi, F. W. Harrison, B. Moore III, and T. S. Zaccheo," First airborne Laser Remote Measurements of Atmospheric Carbon Dioxide, Presented at Fourth Symposium on Lidar Atmospheric Applications", *89th AMS Annual Meeting*, Phoenix, Arizona, 11-15 January 2009c.
31. J. Dobler, M. Dobbs, S. Zaccheo, J. Nagel, W. Harrison, E. Browell, B. Moore, B., "CW fiber laser absorption spectrometer for O₂ column measurements in support of the ASCENDS Mission, The 89th AMS Annual Meeting, Phoenix, Arizona, 11-15 January 2009.
32. M. Dobbs, W. Krabill, M. Cisewski, F. W. Harrison, C. K. Shum, D. McGregor, M. Neal, and S. Stokes, "A multifunctional fiber laser lidar for Earth science and exploration",

- Proceedings of Earth Science Technology Conference, College Park, MD, 24-26 June 2008.
33. Stanford Research Systems, “About Lock-in Amplifiers” Application Note. Sunnyvale, CA, 1999 (Available at http://www.srsys.com/html/application_notes.html. A functional description of lock-in amplifiers).
 34. M.L. Simpson, M. Cheng, T.Q. Dam, K.E. Lenox, J.R. Price, J.M. Storey, E.A. Wachter, and W.G. Fisher, “Intensity-modulated, stepped frequency cw lidar for distributed aerosol and hard target measurements,” *Appl. Opt.* 44, 7210 (2005).
 35. Masaharu I., S. Kameyama, Y. Hirano, S. Ueno, D. Sakaizawa, S. Kawakami, and M. Nakajima, “Laser absorption spectrometer using frequency chirped intensity modulation at 1.57 μm wavelength for CO₂ measurement”, *Opt.Lett.*, 37, 2688-2690, (2012).
 36. Kuze, A., D. M. O’Brien, T. E. Taylor, J. O. Day, C. W. O’Dell, F. Kataoka, M. Yoshida, Y. Mitomi, C. J. Bruegge, H. Pollock, R. Basilio, M. Helmlinger, T. Matsunaga, S. Kawakami, K. Shiomi, T. Urabe, and H. Suto, “Vicarious calibration of the GOSAT sensors using the Railroad Valley desert playa”, *IEEE Trans. Geosci. Remote Sens.*, 49, 1781-1795, doi:10.1109/TGRS.2010.2089527 (2011).
 37. Y. Hu, K. Stamnes, M. Vaughan, J. Pelon, C. Weimer, C. Wu, M. Cisewski, W. Sun, P. Yang, B. Lin, A. Omar, D. Flittner, C. Hostetler, C. Trepte, D. Winker, G. Gibson, and M. Santa-Maria, “Sea surface wind speed estimation from space-based lidar measurements”, *Atmos. Chem. Phys.*, 8, 3593-3601 (2008).
 38. Y. Choi, S. Vay, K. Vadrevu, A. Soja, J. Woo, S. Nolf, G. Sachse, et. Al., “Characteristics of the atmospheric CO₂ signal as observed over the conterminous United States during INTEX NA”, *J. Geophys. Res.*, 113, D07301, doi:10.1029/2007JD008899 (2008).

39. S. Vay, J. Woo, B. Anderson, et al., "Influence of regional-scale anthropogenic emissions on CO₂ distributions over the western North Pacific", *J. Geophys. Res.*, 108, D20, 8801, doi:10.1029/2002JD003094 (2003).
40. HITRAN 2008 database, <http://cfa-www.harvard.edu/hitran/>
41. Devi, V. M., Benner, D. C., Brown, L. R., Miller, C. E., Toth, R. A., "Line mixing and speed dependence in CO₂ at 6348 cm⁻¹: Position, intensities, and air- and self-broadening derived with constrained multispectrum analysis", *JMS*, 242, 90-117 (2007)
42. GLOBE Task Team and others (Hastings, D.A., P.K. Dunbar, G.M. Elphinstone, M. Bootz, H. Murakami, H. Maruyama, H. Masaharu, P. Holland, J. Payne, N. A. Bryant, T.L. Logan, J.-P. Muller, G. Schreier, and J. MacDonald), eds., "The Global Land One-kilometer Base Elevation (GLOBE) Digital Elevation Model", Version 1.0. National Oceanic and Atmospheric Administration, National Geophysical Data Center, 325 Broadway, Boulder, Colorado 80303, 1999. (U.S.A. Digital data base on the World Wide Web; [URL: http://www.ngdc.noaa.gov/mgg/topo/globe.html](http://www.ngdc.noaa.gov/mgg/topo/globe.html)).
43. E. Browell, J. Dobler, S. Kooi, M. Fenn, Y. Choi, S. Vay, F. W. Harrison, B. Moore III, and T. S. Zacheo," Validation of Airborne CO₂ Laser Measurements", Presented at 5th Symposium on Lidar Atmospheric Applications, 91st AMS Annual Meeting, Seattle, Washington, 23-28 January 2011.
44. Cook, C. & Bernfeld, M. "Radar Signals: An Introduction to Theory and Application", (Academic Press, ISBN 0-89006-733-3, New York, 1967)
45. Anatoliy Kononov, Lars Ulander and Leif Eriksson. "Design of Optimum Weighting Functions for LFM Signals", *Convergence and Hybrid Information Technologies*, Marius Crisan (Ed.), ISBN: 978-953-307-068-1, InTech, Available from:

<http://www.intechopen.com/books/convergence-and-hybrid-informationtechnologies/design-of-optimum-weighting-functions-for-lfm-signals>, (2010).

Table 1. Key MFL Instrument Parameters

Seed laser type:	DFB diode laser FITELE FOL15DCWD
Line width	< 6 MHz each wavelength
Side mode suppression ratio:	>45 dB
CO ₂ lines: (vacuum)	1571.112 nm (On), 1571.061 nm (Off 1), 1571.161 nm (Off 2)
Altimetry line: (vacuum)	1596 nm
Modulator:	Semiconductor Optical Amplifiers, Covega BOA1080
Modulation Type:	Intensity modulated continuous wave (IM-CW)
Optical amplifier:	IPG EAD-5L EDFA CO ₂ , IPG EAD-5L EDFA Altimetry
Output power:	5 Watts (Total for CO ₂ wavelengths 3:2:1 ratio On, Off1, Off 2) and 5 W for the altimeter wavelength (simultaneous transmission and reception of all wavelengths)
Bandpass filter width:	2.4 nm CO ₂
Telescope (shared with Altimeter):	Simple 8 in. diam. parabola, F/3, fiber coupled with ~1.5 in. center obscuration, 365 μm fiber core with 0.22 NA
Detectors:	HgCdTe APD, 0.5 mm X 0.5 mm CO ₂ DRS - A3051 44 of 64 good diodes in parallel, Newport 818-BB InGaAs PIN CO ₂ reference channel, Hamamatsu H10330 PMT Altimeter
Detector Coll. Eff.:	0.50 CO ₂ accounting for bad diodes, 0.04 Altimeter
Detector gain:	~940 with excess noise factor ~1.3, 77 K as operated, altimeter (adjustable)
Transimpedance Amplifier:	Femto HCA-2M-1M gain 10 ⁶ CO ₂ science channel and 10 ³ reference
Analog Filter:	1P- HP 3.5 kHz, 3P-LP 2 MHz
Analog IO:	NI PXIe-6368
Sample Rate:	2 Ms/sec
Encoding Scheme:	Swept-frequency; ~350 KHz ± 250 KHz (CO ₂) 2011 Rolling tones; 50 KHz ± ~3 KHz (CO ₂) 2009-2010 Pseudo-Noise (PN) (Altimeter)
Maximum Unambiguous Range:	15-km -200 samples (Selectable) CO ₂
Laser divergence angle:	190 urad (half angle)
Receiver FOV:	240 urad (half angle)
Receiver recording duty cycle:	100%
Reporting interval:	100 msec (10 Hz)

--	--

Table 2. Surface Reflectance and CO₂ Measurement Precision during 2010 ASCENDS DC-8 Campaign.

Surfaces	Desert	Desert	Vegetation	Vegetation	Ocean³
Location	Railroad Valley, NV	Needles, CA	Central Valley, CA	DOE ARM, Lamont, OK	Pacific off Baja
Median Surface Reflectance¹ [sr⁻¹]	0.143	0.118	0.098	0.080	0.019 (0.03-0.06)⁴
1-s CO₂ SNR² (CO₂ [ppmv])	630 (0.59)	612 (0.59)	545 (0.68)	560 (0.65)	~186 (2.07)
10-s CO₂ SNR² (CO₂ [ppmv])	1347 (0.27)	1443 (0.25)	1236 (0.30)	1460 (0.25)	~531 (0.72)

¹ Reflectance values normalized to Railroad Valley.

² SNR estimated for 7-km altitude.

³ Low estimate in 2010 likely due to poor alignment.

⁴ Values from 2009 campaign.

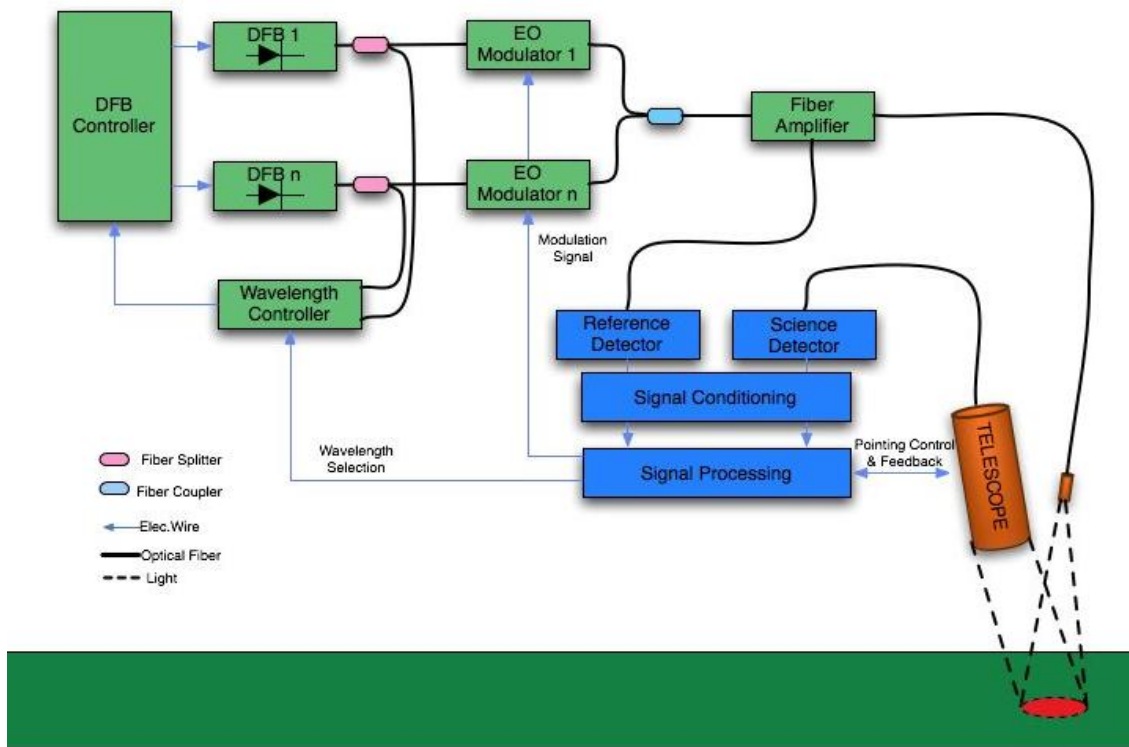


Figure 1. MFLL conceptual architecture.

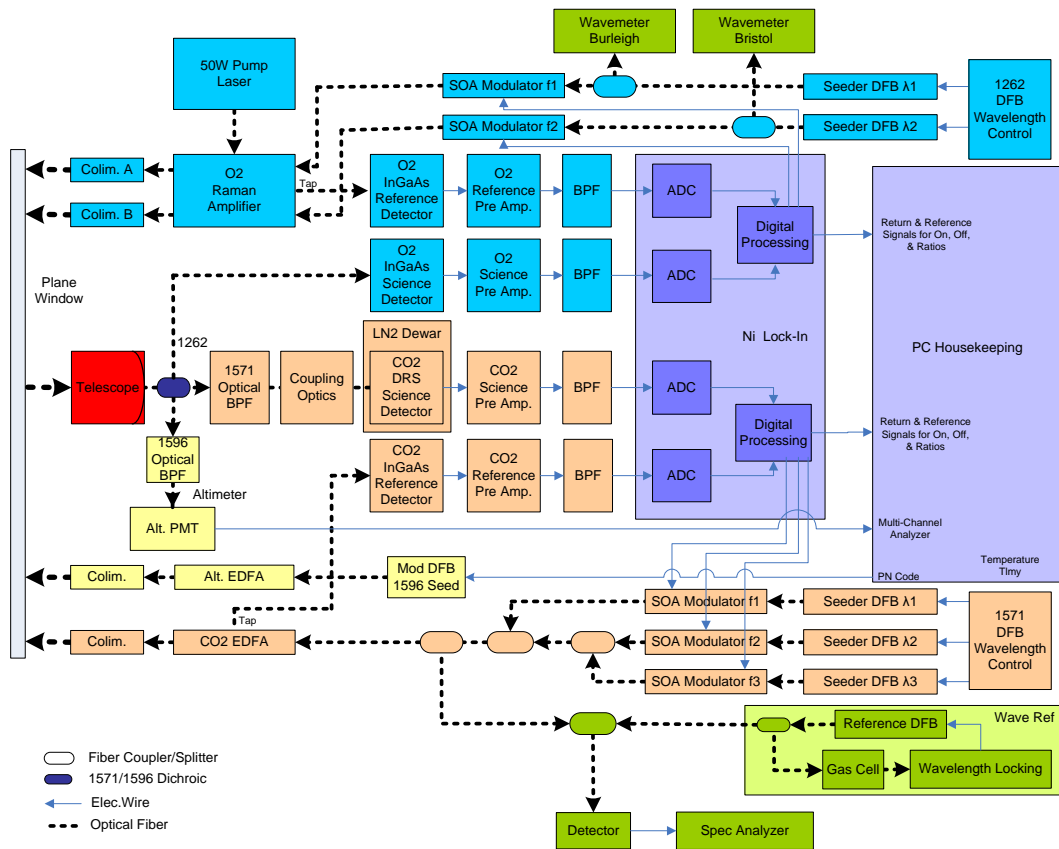


Figure 2. Basic block diagram of MFL instrument as flown in 2011



Figure 3. Summary of MFL flight test campaigns.

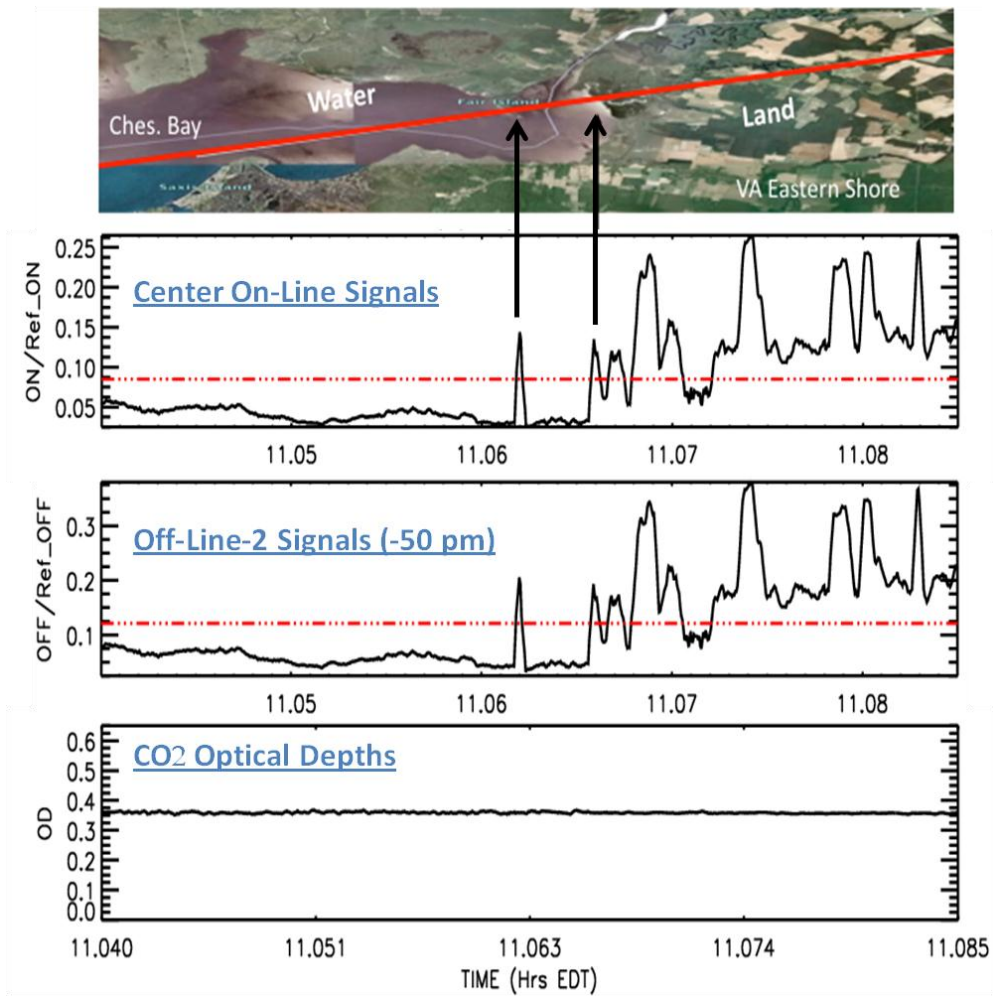


Figure 4. MFL flight test on 22 October 2007 showing water-to-land transition. It shows the flight track in solid red line; and energy normalized on and off signals and OD measurements

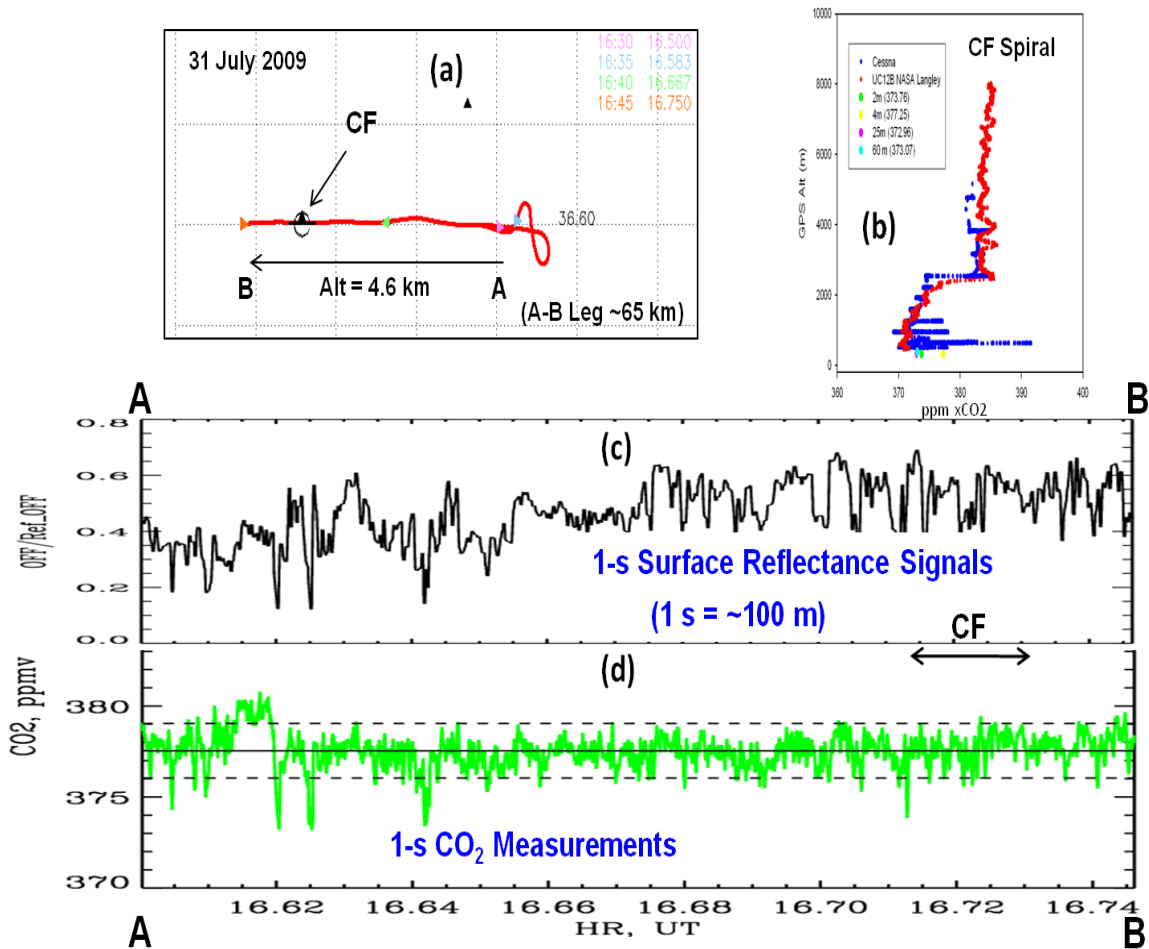


Figure 5. MFL measurements made over the Department of Energy Atmospheric Radiation Measurement (DOE/ARM) Central Facility from an altitude of 4.6 km on 31 July 2009; (a) shows the flight track; (b) shows the *in situ* measured CO₂ profile over the CF in red along with the CO₂ profile measured earlier on a DOE Cessna aircraft shown in blue and a tower CO₂ measurement shown in green; (c) shows the off-line surface reflectance signals with 1-s averaging from A to B; and (d) shows the variation in CO₂ OD measurements in terms of XCO₂. The leg-averaged column XCO₂ is shown in (d) by the solid line, and dashed lines are ± 1.5 ppmv.

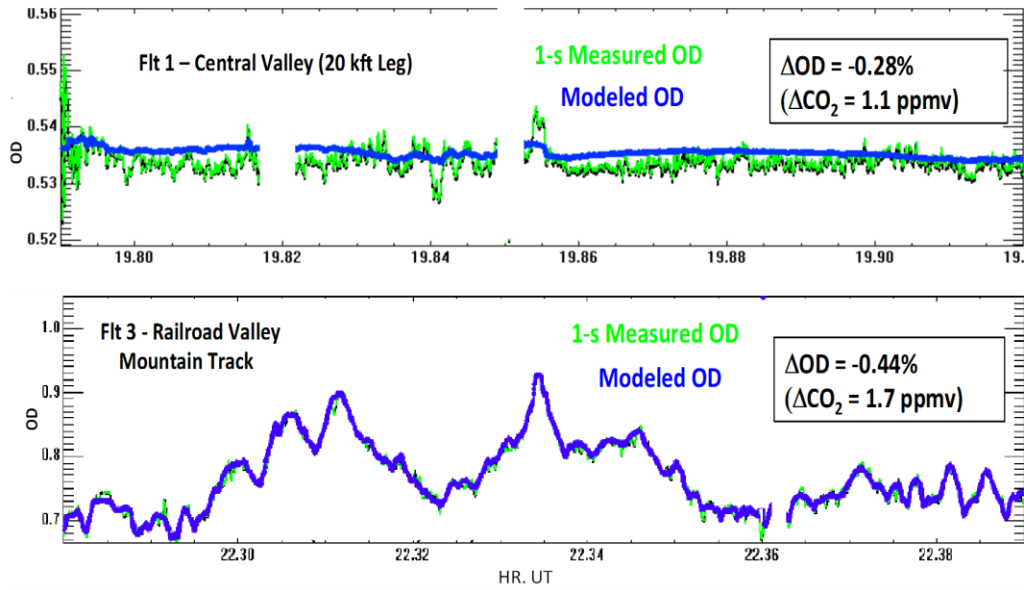


Figure 6. Comparison of MFLM measured and modeled CO₂ optical depths (OD's) on DC-8 flights over California's Central Valley (top) and Rocky Mountains (bottom) in route to Railroad Valley (RRV), NV.

Flt#	Range	!CO2
0	3147	0.6
	6363	0.3
	9583	2.0
	12738	-1.9
1	4801	-3.4
	4889	-2.0
	6408	-2.7
	8012	2.6
	9605	1.6
	11196	0.6
	12806	1.7
3	4825	-1.6
	3329	-2.3
	4918	-2.6
	4982	0.2
	6593	2.9
	8179	1.2
	9354	-3.0
5	11362	-0.3
	3116	-0.5
	3107	-1.2
	4826	0.2
6	8056	-2.3
	11214	-1.0
	2891	-3.0
	4478	-0.6
	6053	-0.6
	7649	0.2
7	9209	-1.9
	10747	-1.4
	12326	-0.2
	4499	0.6
	4222	-1.8
	5806	-2.0
	7367	1.1
8930	1.3	
10465	-2.7	
11829	-2.4	

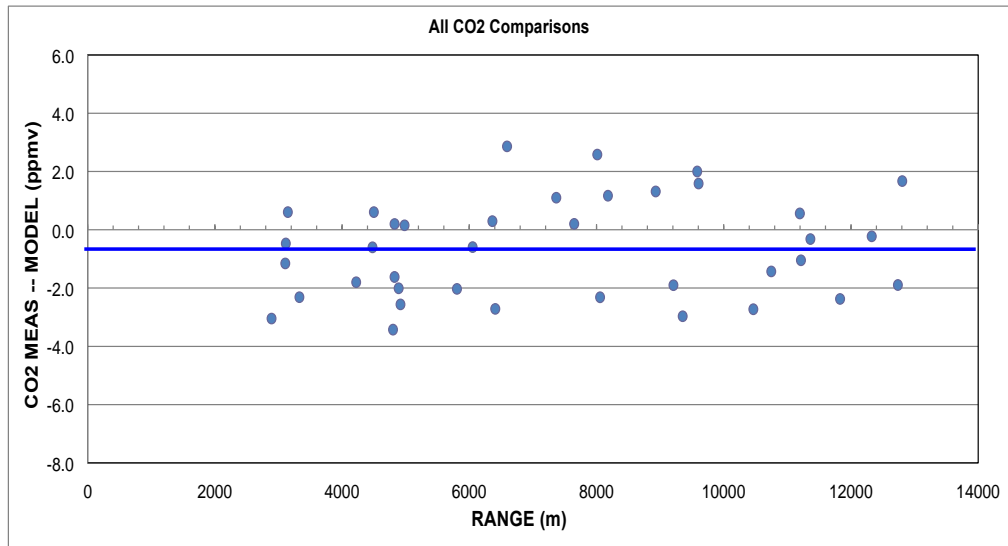


Figure 7. Comparison of measured and modeled CO₂ OD's expressed in terms of equivalent XCO₂ from six flights during the 2011 ASCENDS DC-8 Campaign. The data for each of the flights is shown in the table along with range to flight levels, and measured – model XCO₂ differences (!CO₂). The location and dates of the flights are: Flt. 0: Central Valley, CA, 26 July; Flt. 1: Central Valley, CA, 28 July; Flt. 3: Railroad Valley, NV, 3 August; Flt. 5: Four Corners, NM, 9 August; Flt. 6: NOAA WBI Tall Tower at West Branch, IA, 10 August; Flt. 7: NOAA LEF Tall Tower at Park Falls, WI, 11 August. The

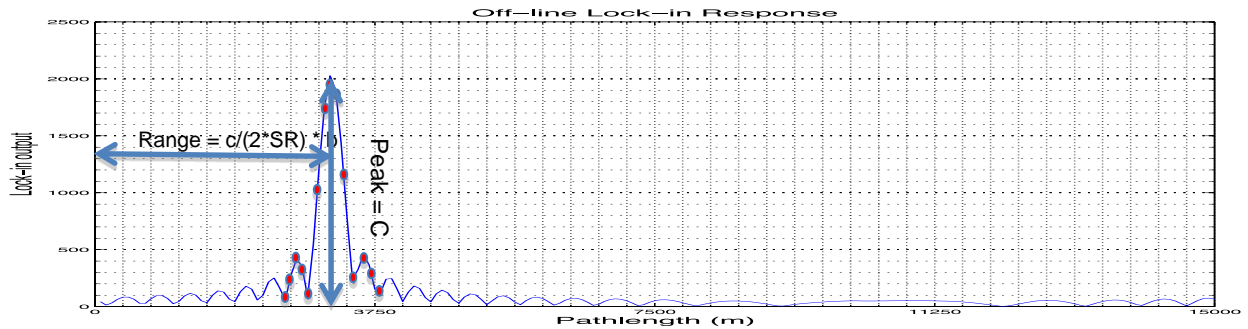


Figure 8. Sampled output of the lock-in processor is illustrated in red and Equation 14 fitted to the lock-in output in blue. Only at integer multiples of the sample period is the amplitude of the lock-in output and the estimate of the amplitude (C) provided by the fit of Equation 14 match. At all other correlation delays, the amplitude of the sampled correlation is less than the true amplitude. Range is a function of the delay to the peak of the fit.

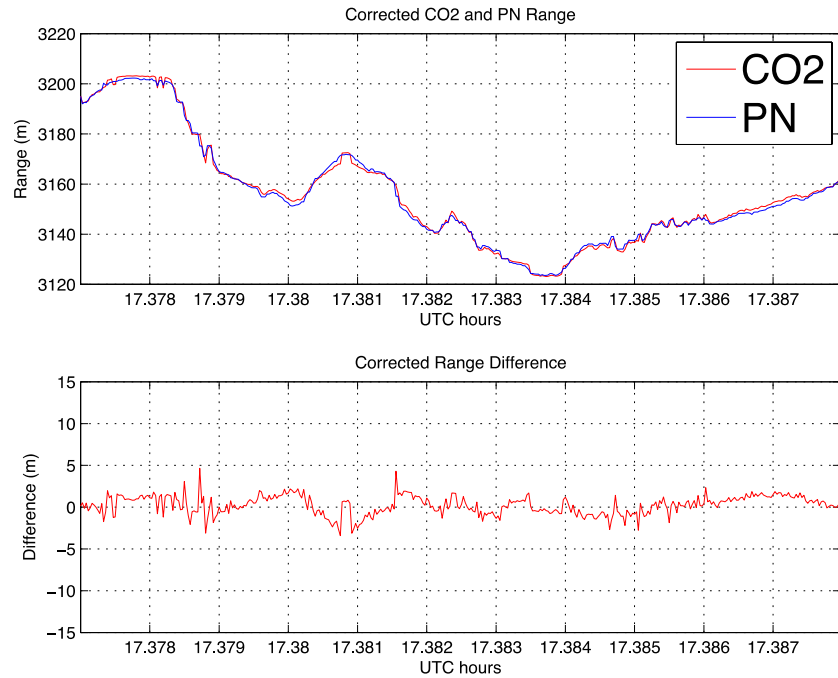


Figure 9. Range estimates obtained from the off-line CO₂ return and time coincident returns from the on-board PN altimeter over the four corners region from the DC-8 on 7 August 2011. Sum Square Error (SSE) over this interval is 1.35 meters. Mean difference = 0.2302 m with a STD of 1.4418 m.

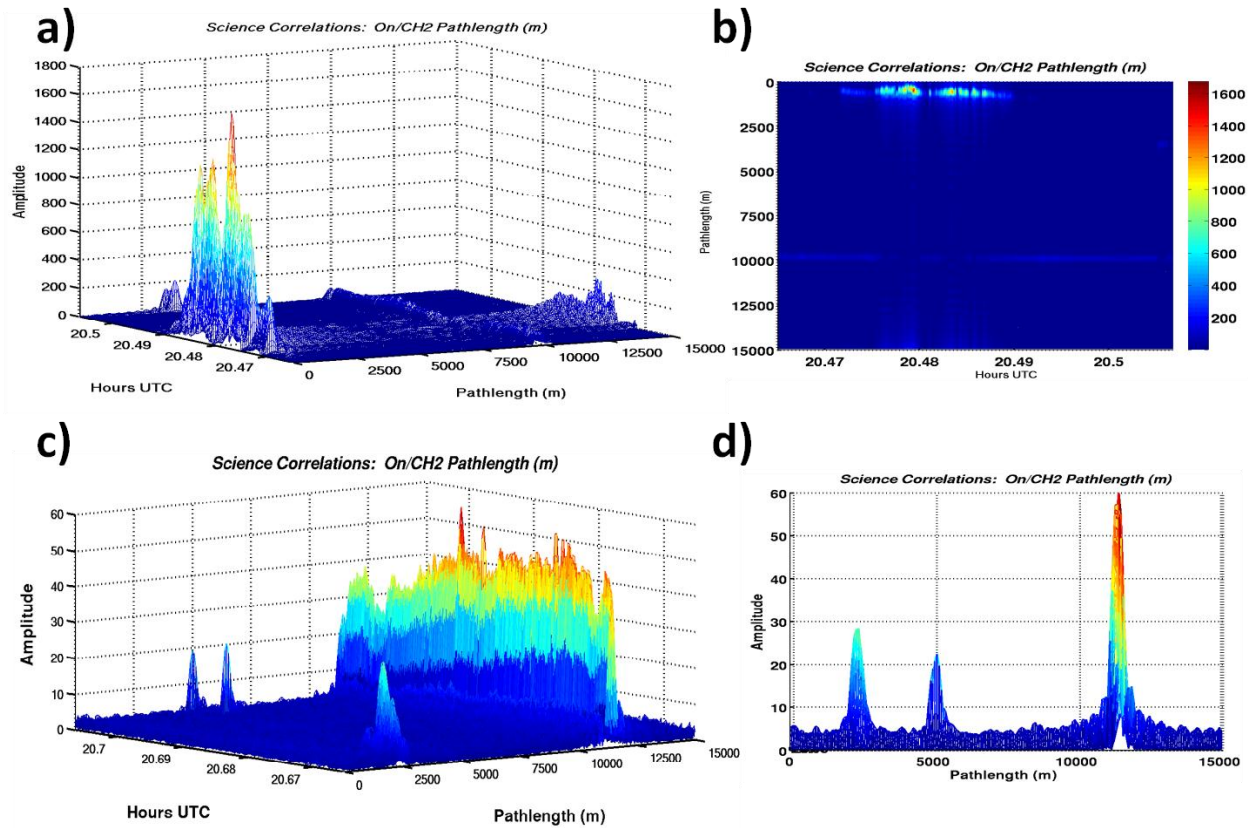


Figure 10. Examples of flight data showing the range discrimination of cloud returns from ground returns using the swept frequency IM-CW approach from the DC-8 on 04 August 2011. Panel a) shows a 3-D representation of a large cloud return above a small ground return and panel b) is the projection of the information in a) onto a 2-D image of signal profiles along the flight track illustrating the strong cloud and weak ground returns; panel c) slows the distribution of signals from weak clouds and strong ground return signals and panel d) is a superposition of data from c) on a signal vs pathlength grid.